JGR Oceans

RESEARCH ARTICLE
10.1029/2018JC014794

This article is a companion to Toggweiler et al. (2019), https://doi.org/10.1029/2018JC014795.

Key Points:
- Low-delta^{14}C surface waters are found in upwelling zones along the margins and in the subarctic Pacific gyre
- The low-delta^{14}C water in most of the upwelling zones appears to be mode or intermediate water from the ACC
- The volumes of upwelling in these areas exceed the volumes that would be drawn up to the surface by the local winds

Supporting Information:
- Supporting Information S1
- Table S4
- Table S5
- Table S6
- Data Set S1

Correspondence to:
J. R. Toggweiler,
robbie.toggweiler@noaa.gov

Citation:
Toggweiler, J. R., Druffel, E. R. M., Key, R. M., & Galbraith, E. D. (2019). Upwelling in the ocean basins north of the ACC: 1. On the upwelling exposed by the surface distribution of Δ^{14}C. *Journal of Geophysical Research: Oceans*, *124*, 2591–2608. https://doi.org/10.1029/2018JC014794

Received 26 NOV 2018
Accepted 28 FEB 2019
Accepted article online 4 MAR 2019
Published online 29 APR 2019

Upwelling in the Ocean Basins North of the ACC: 1. On the Upwelling Exposed by the Surface Distribution of Δ^{14}C

J. R. Toggweiler[1], Ellen R. M. Druffel[2], Robert M. Key[3], and Eric D. Galbraith[4,5]

[1]Geophysical Fluid Dynamics Laboratory, NOAA, Princeton, NJ, USA, [2]Department of Earth System Science, University of California, Irvine, Irvine, CA, USA, [3]Atmospheric and Oceanic Sciences Program, Princeton University, Princeton, NJ, USA, [4]ICREA, Barcelona, Spain, [5]ICTA, Universitat Autonoma de Barcelona, Barcelona, Spain

Abstract The upwelling associated with the ocean's overturning circulation is hard to observe directly. Here, a large data set of surface Δ^{14}C measurements is compiled in order to show where deep water is brought back up to the surface in the ocean basins north of the Antarctic Circumpolar Current (ACC). Maps constructed from the data set show that low-Δ^{14}C deep water from the ACC is drawn up to the surface in or near the upwelling zones off Northwest Africa and Namibia in the Atlantic, off Costa Rica and Peru in the Pacific, and in the northern Arabian Sea in the Indian Ocean. Deep water also seems to be reaching the surface in the subarctic Pacific gyre near the Kamchatka Peninsula. The low-Δ^{14}C water drawn up to the surface in the upwelling zones is also shown to spread across the ocean basins. It is easily seen, for example, in the western Atlantic off Florida and in the western Pacific off New Guinea and Palau. The spreading allows one to estimate the volumes of upwelling, which, it turns out, are similar to the volumes of large-scale upwelling derived from inverse box models. This means that very large volumes of cool subsurface water are reaching the surface in and near the upwelling zones—much larger volumes than would be expected from the local winds.

Plain Language Summary The deep layers of the ocean are filled with cold dense water that sinks from the surface near Antarctica and in the northern North Atlantic. This process is understood reasonably well. The countervailing process—the way that the dense water is brought back up to the surface—is not as well understood. Oceanographers now agree that the ocean's deep water is drawn back up to the surface ("upwelled") mainly around Antarctica as part of the wind-driven overturning in the Antarctic Circumpolar Current (ACC). But cool water is also known to reach the surface in upwelling zones around the ocean's margins. Here we map the upwelling north of the ACC with the radioactive isotope carbon-14 and show that the deep water upwelled to the surface around Antarctica seems to be drawn up to the surface a second time in the upwelling zones. The water drawn up to the surface in the upwelling zones then flows back to the North Atlantic and sinks again to complete the cycle.

1. Introduction

^{14}C is a radioactive isotope that is produced in the atmosphere and decays primarily in the ocean. The ocean is therefore deficient in ^{14}C in relation to the atmosphere. Oceanic ^{14}C deficits have long been used to establish an age or turnover time for the water in the deep ocean.

Here we consider a less well-known ^{14}C application—the deficits at the ocean's surface. Our goal is to see what surface ^{14}C deficits can reveal about the upwelling portion of the ocean's overturning circulation. We are aided in this task by the fact that the ^{14}C deficits in upwelled water can persist at the surface for 10 years or more owing to the slow gas exchange process for ^{14}C (Broecker & Peng, 1974).

^{14}C is reported as Δ^{14}C, the per mil departure of the measured ^{14}C/^{12}C ratio in a sample from a standard reference ratio after a correction for isotopic fractionation (Stuiver & Polach, 1977). The reference ratio is the atmospheric ^{14}C/^{12}C ratio during the late nineteenth century. The ocean's surface waters had an average deficit of about 50‰ before the nuclear weapons tests of the 1950s and early 1960s (Broecker & Peng, 1982). Some areas of the ocean had smaller deficits while other areas had larger deficits, most notably the areas near Antarctica.

The ocean's overturning is now thought to consist of two counterrotating meridional cells that are called, somewhat prosaically, the “lower cell” and the “upper cell” (Lumpkin & Speer, 2007; Speer et al., 2000). The upwelling in both cells occurs along the sloping isopycnals of the Antarctic Circumpolar Current (ACC) around Antarctica (Marshall & Speer, 2012). The deep water that reaches the surface via the lower cell flows to the south and sinks again to become Antarctic bottom water. The focus here is on the deep water that reaches the surface via the upper cell, which eventually becomes deep water again in the North Atlantic.

The deep water drawn up to the surface via the upper cell moves away from Antarctica initially in the surface Ekman layer. It then combines with water from the subtropical gyres and drops below the surface again as the mode and intermediate waters that are formed along the northern flank of the ACC (Iudicone et al., 2008; Sloyan et al., 2010). Inverse box models suggest that 8–10 Sv of water in this density class is drawn up to the surface again in the tropical Atlantic and eastern Pacific (Lumpkin & Speer, 2003; Sloyan et al., 2003; Wunsch, 1984). The inverse models are not very specific, however, about how and where the upwelling takes place.

Our goal in this paper is to map the surface distribution of $\Delta^{14}C$ in order to determine where the upwelling north of the ACC occurs. The task is nominally fairly simple: Find the surface waters with the lowest $\Delta^{14}C$ values; the areas with the lowest $\Delta^{14}C$ should be the areas of upwelling. Indeed, the lowest $\Delta^{14}C$ values are found in or near the upwelling zones off Peru and Kamchatka in the Pacific, off Northwest Africa and Namibia in the Atlantic, and in the northern Arabian Sea in the Indian Ocean. This will seem odd to most oceanographers because the upwelling in these areas is thought to come from relatively shallow depths and is not usually associated with the ocean's large-scale overturning.

The present paper is focused on the $\Delta^{14}C$ measurements and the construction of the maps. It begins with a brief review of the upwelling off Peru (section 2). The bomb ^{14}C problem is discussed in sections 3 and 4. Our maps are presented in sections 5–7. A companion paper by the same authors (Toggweiler et al., 2019) takes up the question of how the upwelling occurs.

2. Peru Upwelling

A precursor for this study was carried out by Toggweiler et al. (1991), hereon TDB91. TDB91 used the surface $\Delta^{14}C$ to examine the upwelling in a vintage circulation model from the 1980s. They were able to draw on eight “prebomb” observations from the tropical Pacific to test the model.

The overturning in the model delivered deep water up into the thermocline, which was then funneled up to the surface along the equator via the equatorial divergence. The model therefore predicted that the surface waters near the equator would be low in $\Delta^{14}C$. TDB91 showed, however, that the water upwelled via the equatorial divergence is not low $\Delta^{14}C$ and argued that all the low-$\Delta^{14}C$ water in the equatorial zone comes from the area off Peru instead. TDB91 then traced the water off Peru back to the Subantarctic Mode Water (SAMW) that forms along the ACC in the South Pacific.

This result was consistent with the idea, new at the time, that deep water is drawn up to the surface around Antarctica and spreads to the north below the thermocline on its way back to the North Atlantic (Sloyan & Rintoul, 2001; Talley, 2008; Toggweiler & Samuels, 1993). In this context, TDB91 showed that the subantarctic water on its way back to the North Atlantic is drawn up to the surface a second time off Peru.

The SAMW-Peru connection is not immediately obvious because the water upwelling off Peru is warmer than SAMW. This led TDB91 to argue that SAMW is warmed a few degrees by mixing during a long traverse from the ACC; they also showed how the same mixing would have a small effect on the $\Delta^{14}C$ due to the weak coupling between the $\Delta^{14}C$ contents of the atmosphere and upper ocean during prebomb time. The insensitivity to mixing makes $\Delta^{14}C$ a better indicator of the origin of the water. (For more information on this point, the reader should consult the discussion related to Figure 16 in TDB91).

TDB91 were able to determine that the SAMW in the South Pacific had a prebomb $\Delta^{14}C$ of −76 to −81‰. This range compared favorably with the $\Delta^{14}C$ values in a coral from the Galapagos Islands (Druffel, 1981). With the larger data set in this paper, we can now say that the −76 to −81‰ range seems to characterize the surface $\Delta^{14}C$ in all the upwelling areas where prebomb measurements are available.

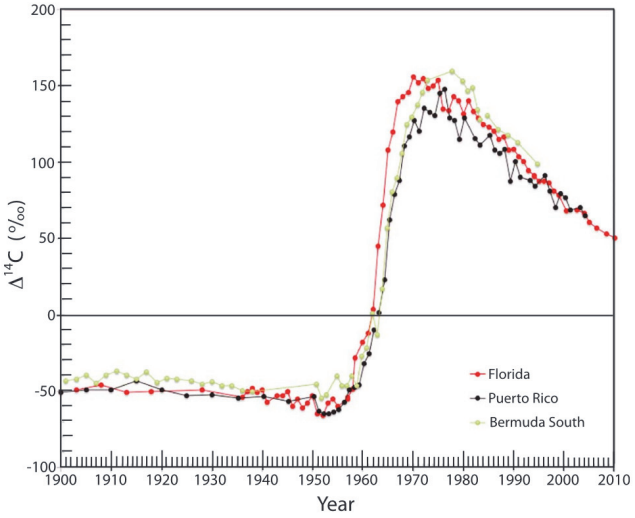

Figure 1. Surface $\Delta^{14}C$ recorded by three Atlantic corals. The records are from the Florida Keys (Druffel & Linick, 1978; Druffel unpublished), the south coast of Puerto Rico (Kilbourne et al., 2007), and the south coast of Bermuda (Druffel, 1989; Goodkin et al., 2012).

SAMW is a mixture of upwelled deep water from the area south of the ACC and upper-ocean water from the subtropical gyres (Iudicone et al., 2008). In this regard, TDB91's −76 to −81‰ range lies about half way between the prebomb $\Delta^{14}C$ values in the polar surface waters south of the ACC and in the subtropical waters north of the ACC.

3. Anthropogenic Perturbations

Relatively few observations were available to TDB91 because of the nuclear weapons tests that took place in the 1950s and early 1960s. The bomb tests added a spike of new ^{14}C atoms to the atmosphere that altered the steady state distribution before the bomb tests. Most of what is known about $\Delta^{14}C$ in the ocean comes from seawater samples that were collected after the bomb tests. TDB91 drew upon corals and shells that grew in the ocean before the bomb tests had begun.

The bomb tests also occurred in the midst of a slow, long-term decline in the surface $\Delta^{14}C$ due to the burning of fossil fuels. Figure 1 shows the fossil fuel and bomb perturbations in three corals from the North Atlantic. The average $\Delta^{14}C$ at the three locations was about −45‰ in 1900. The surface $\Delta^{14}C$ then declined to −55‰ during the first half of the twentieth century due to the burning of fossil fuels. The invasion of bomb ^{14}C into the ocean began about 1955. The surface $\Delta^{14}C$ then jumped up dramatically and reached +150‰ during the 1970s. The first ocean-wide survey of $\Delta^{14}C$ took place around this time (Broecker et al., 1985).

A much more detailed survey was carried out 20 years later as part of the World Ocean Circulation Experiment (WOCE). Figure 2 shows the surface $\Delta^{14}C$ values in the Pacific Ocean during WOCE. The highest $\Delta^{14}C$ values (red shades) are along 30°N and 30°S. The lowest values (dark blue shades) are along the southern edge of the map at 60°S and in the northwest near Kamchatka. The lowest values in the tropical Pacific (green shades) are south of the equator and close to Peru.

The WOCE surveys took place at an opportune time with respect to $\Delta^{14}C$. In 1965, shortly after the end of the bomb tests, the $\Delta^{14}C$ gradient between the atmosphere and surface ocean peaked at about 700‰. ^{14}C was flooding into the ocean at this time. By 1990, the average atmosphere–ocean gradient had fallen back to 50‰, that is, the same gradient that prevailed during prebomb time (Figure 5 in Druffel et al., 2010). But the gradient continued to shrink due to the ongoing burning of fossil fuels. After 2000, the $\Delta^{14}C$ of the atmosphere began to fall below the surface $\Delta^{14}C$ levels in many parts of the ocean and ^{14}C stopped entering the ocean in those areas. So the WOCE surveys took place at a time *between* the bomb era and the fossil fuel era when ^{14}C was entering the ocean at the same low rates that prevailed during prebomb time.

Here, information is compiled from dozens of new coral and shell locations to produce a prebomb data set that can be directly compared to the WOCE data set. The spatial patterns during the two time periods are found to overlap very well. The focus here will be on three time windows with the largest numbers of measurements. These are the prebomb period, 1940–1954, the WOCE era, 1990–1994, and the fossil fuel-dominated CLIVAR era, 2003–2007, Climate and Ocean: Variability, Predictability and Change.

4. Deficit Maps

The measurement errors for $\Delta^{14}C$ are not small in relation to the features considered in this paper. The error for an individual sample varies from 2‰ to 7‰. Seawater observations also tend to be fairly noisy because they are subject to weather-related water mass changes (McDuffee & Druffel, 2007) and to seasonal mixing with subsurface waters (Druffel et al., 2010).

To improve the signal-to-noise ratio, we have identified 143 “regions of interest” where multiple $\Delta^{14}C$ measurements are available. All the measurements from a given region and time period are averaged together. The regional averages are then normalized by subtracting the contemporary $\Delta^{14}C$ value from

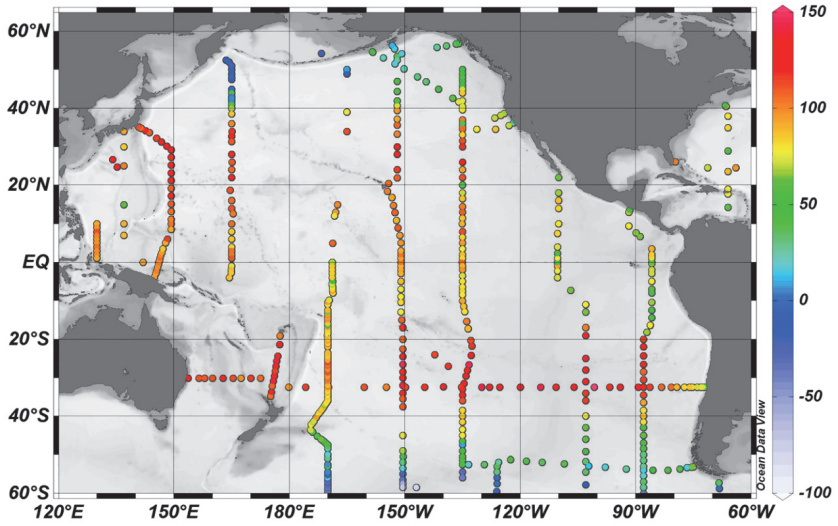

Figure 2. Surface distribution of $\Delta^{14}C$ for the Pacific Ocean from seawater samples collected between 1991 and 1996 during the World Ocean Circulation Experiment.

Okinawa in the western North Pacific. Our maps are constructed from these differences—called "deficits" from here on.

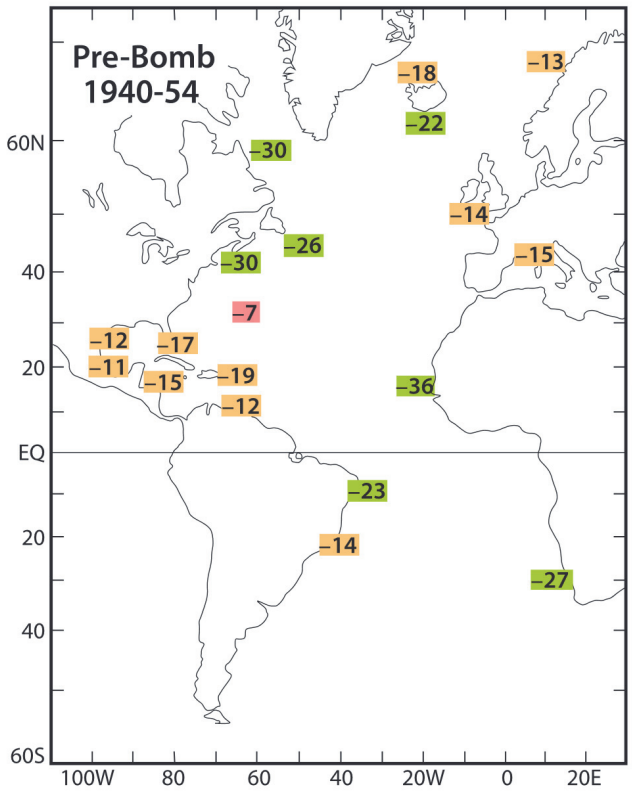

Figure 3. $\Delta^{14}C$ deficits in the Atlantic during prebomb time (1940–1954). Okinawa reference = −41‰. The deficits with orange backgrounds range from −11 to −20. The deficits with green backgrounds are larger (more negative) than −20.

The normalization highlights the fact that the $\Delta^{14}C$ differences across the ocean basins are similar during all three time periods. The differences on our maps are mostly negative (deficits), because most areas of the ocean are lower in $\Delta^{14}C$ than Okinawa.

More details about the normalization and the observations within each region can be found in the Supporting Information S1. Each of our regions is given a number. Okinawa, for example, is Region 18 in the Pacific (Table S2). It had a prebomb $\Delta^{14}C$ of −41‰ (Table S5) and has a deficit of zero, by definition. The area off Peru is Region 45. According to TDB91, the SAMW upwelling off Peru should have had a prebomb $\Delta^{14}C$ of −76 to −81‰. Subtracting −41‰ (for Okinawa) leads us to expect a deficit of −35 to −40.

Our deficit maps for the Atlantic are shown below in Figures 3–5. Our maps for the Pacific are shown in Figures 6–8, and those for the Indian are shown in Figures 9 and 10. The deficits on the maps are divided into four sizes, small, medium, large, and extra large and are color coded accordingly. Small deficits have a red background. They are typically found within the subtropical gyres. Extra large deficits have a blue background and are generally confined to the subpolar zones. Our medium and large deficits have orange and green backgrounds, respectively.

Our maps are meant to show how the surface $\Delta^{14}C$ is influenced by the time-mean circulation and overturning. To be sure, the $\Delta^{14}C$ at a particular time and location is also influenced by the temporal variability of the circulation itself and by the temporal changes associated with the bomb transient. The $\Delta^{14}C$ is also subject to measurement error. Nevertheless, the impact of the time-mean overturning seems quite clear when our maps are considered together. The areas of upwelling stand out, in particular, as areas with persistently low values across all three time periods.

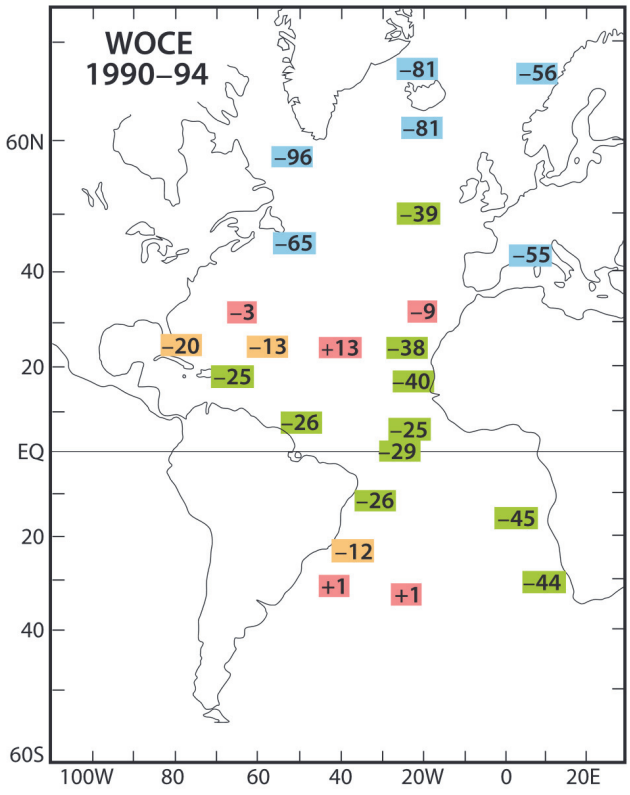

Figure 4. $\Delta^{14}C$ deficits in the Atlantic during the World Ocean Circulation Experiment (WOCE) era (1990–1994). Okinawa reference = 116‰. The deficits with red backgrounds range from −9 to +13. Orange deficits range from −11 to −20. Green deficits range from −21 to −50. The blue deficits are larger than −50.

5. Deficit Maps for the Atlantic Ocean

5.1. Prebomb Period (1940–1954)

Our deficit map for the Atlantic during the prebomb period appears in Figure 3. All the measurements used to make this map are from corals and shells. There is only one small (red) deficit on the map, the −7 value from Bermuda.

The largest deficit on the map is the −36 (green) value off northern Africa. This value comes from four shells collected in the core area of the Northwest Africa Upwelling Zone (Chavez & Messié, 2009; Ndeye, 2008). The water upwelling in the area is known to have a South Atlantic origin (Mittelstaedt, 1983; Pastor et al., 2012). The −36 value falls within the −35 to −40 range expected for SAMW.

A deficit of −27 also appears off South Africa. This value comes from a shell collected several hundred kilometers to the south of the core area of the Benguela Upwelling Zone off Namibia (Dewar et al., 2012; Hardman-Mountford et al., 2003; Nelson & Hutchings, 1983). Additional data from this area during 2011–2015 show that the core area of the upwelling zone had a larger deficit at this time than the area off South Africa (see pages 8–9 and Figure S7 in the supporting information).

The map in Figure 3 also includes a number of medium (orange) deficits in the Caribbean Sea and Gulf of Mexico. These values reflect a general pattern that holds in all three ocean basins. Large deficits near the upwelling zones in the east give way to medium-sized deficits in areas far away to the west. The decrease seems to reflect the spreading of water away from the upwelling areas and the impact of gas exchange, which slowly chips away at the deficits from the upwelling areas.

An east-west contrast of opposite sign is found in the northern North Atlantic. The deficits off Norway and Great Britain, in this case, are in the medium range, −13 and −14, respectively. The deficits in the western North Atlantic, meanwhile, clump together around −29. The medium values in the east reflect the impact of gas exchange on the tropical surface waters that are carried northward by the Gulf Stream and the North Atlantic Current. The larger deficits in the west are due to upwelling and/or winter convection in the Slope Sea area north of the Gulf Stream (Tanaka et al., 1990) or in the Labrador Sea.

5.2. WOCE Era (1990–1998)

The WOCE sampling in the Atlantic took place over 9 years, so two maps have been prepared. The main map in Figure 4 is for the years 1990–1994. The second map is for the years 1997–1998; it appears in the supporting information as Figure S5. The Okinawa reference value for the map for 1990–1994 is 116‰.

The main map in Figure 4 has observations from many more locations than the prebomb map in Figure 3. In particular, it includes five small deficits from the subtropical gyres. Three of the small deficits are positive—the local $\Delta^{14}C$ is higher than at Okinawa—most notably the +13 value along 25°N in the middle of the North Atlantic.

A number of the deficits from 1990–1994 are quite similar to the prebomb deficits from the same areas. Bermuda, for example, has a prebomb deficit of −7 and a WOCE deficit of −3. The Florida Keys have a prebomb deficit of −17 and a WOCE deficit of −20. Puerto Rico has a prebomb deficit of −19 and a WOCE deficit of −25, NE Brazil has a prebomb deficit of −23 and a WOCE deficit of −26. SE Brazil has a prebomb deficit of −14 and a WOCE deficit of −12. The similarities show that there is a good correspondence between the deficits during the two time periods in the tropics.

The similarity only holds, however, between 30°N and 30°S. The WOCE map has a number of extra large (blue) deficits in the North Atlantic that are much larger than the deficits in these areas during prebomb

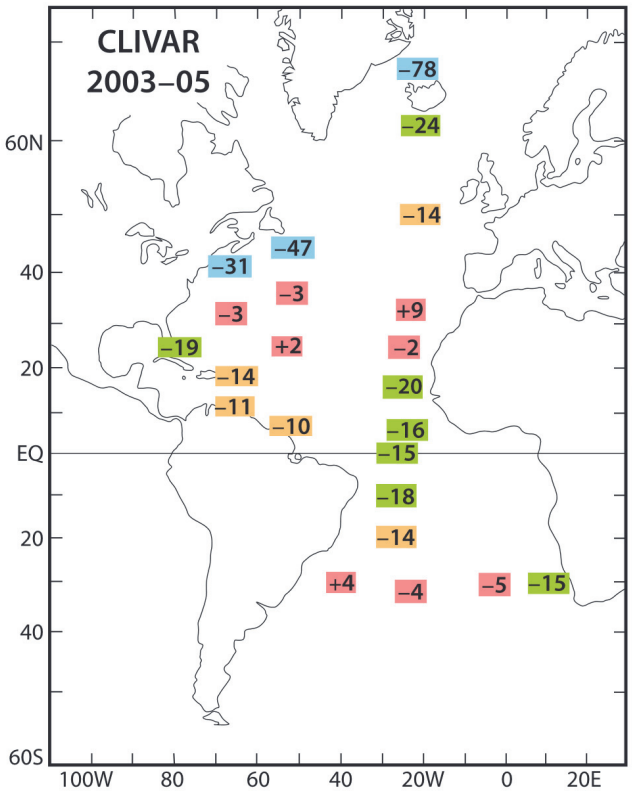

Figure 5. $\Delta^{14}C$ deficits in the Atlantic during the CLIVAR era (2003–2005). Okinawa reference = 84‰. The deficits with red backgrounds range from −5 to +9. Orange deficits range from −10 to −14. Green deficits range from −15 to −30. Blue deficits are larger than −30.

time. A prebomb deficit of −13 off Norway, for example, gives way to a deficit of −56 during WOCE. A prebomb deficit of −15 in the Mediterranean Sea gives way to a deficit of −55 WOCE. These shifts are a consequence of the winter mixing in these areas and the fact that the water mixed up from below remained relatively uncontaminated with bomb ^{14}C into the 1990s.

Again, the most important deficits are the large (green) deficits in the tropical Atlantic. The largest of these are the −44 and −45 values off southern Africa and the −40 value off Northwest Africa. The −40 value off Northwest Africa comes from seven water samples that were collected at different distances from the coast. Four of the seven were collected inshore of the Cape Verde Islands within 250 km of the coast. They would have a deficit of −45 by themselves. The other three samples were collected beyond the Cape Verde Islands about 1,200 km from the coast. The three offshore samples would have a deficit of −33 by themselves.

The deficits on the opposite (eastern) side of the tropical Atlantic range from −26 (NE Brazil and Guiana Current) to −20 (Florida Keys). Two deficits from the equatorial zone, −25 and −29, fall in between. Basically, the whole tropical Atlantic was low in $\Delta^{14}C$ during WOCE. As in the prebomb map, the deficits shrink from east to west. Again, the decline seems to reflect the spreading of the low-$\Delta^{14}C$ water from the coast of Africa and the impact of gas exchange, which chips away at the deficits from the upwelling areas.

The area along the equator has a deficit that is only 3‰ and 4‰ larger than the deficits to the south and north, respectively. These are not significant differences. Like the results in TDB91, they show that the equatorial divergence is not a source of low-$\Delta^{14}C$ water. The deficits in the equatorial zone clearly seem to arise off Africa instead.

5.3. CLIVAR Era (2003–2005)

The Atlantic CLIVAR map in Figure 5 is based on samples collected during 2003–2005. The CLIVAR map has eight small deficits along 30°N and 30°S. The Okinawa reference value for this time period is 84‰.

The range of the deficits during CLIVAR is smaller than the range during WOCE. This reflects the changeover from the bomb era to the fossil fuel era. Sometime around the year 2000 areas like Okinawa stopped taking up ^{14}C from the atmosphere. Bomb ^{14}C, meanwhile, continued reaching the surface from below in the upwelling zones. The combination has reduced the $\Delta^{14}C$ differences across the ocean basins.

The area along the equator has a deficit of −15 during this time period, which is slightly *less* negative than the contemporary deficits to the north and south. Again, these small differences are not significant. They simply reinforce the point made above that the equatorial divergence is not a source of low-$\Delta^{14}C$ water.

The CLIVAR map provides evidence for a large temporal change north of Iceland. During prebomb time the surface waters north and south of Iceland had deficits of −18 and −22, respectively. During WOCE both areas had deficits of −81. As mentioned above, similar changes are seen across the northern North Atlantic and are attributed to winter mixing. During CLIVAR, however, the deficit south of Iceland decreased back to −24 while the deficit north of Iceland remained at −78.

The temporal change would seem to be due to a change in circulation north of Iceland (Scourse et al., 2012). The shelf area north of Iceland is subject to extensive changes as older and fresher polar water from the East Greenland Current and younger, saltier Atlantic water from the Irminger Current take turns dominating the shelf area over time (Eiríksson et al., 2011; Jónsson & Valdimarsson, 2012; Knudsen et al., 2004; Massé et al., 2008). The −78 deficit during CLIVAR may therefore be due to a recent invasion of low-$\Delta^{14}C$ polar water onto the shelf.

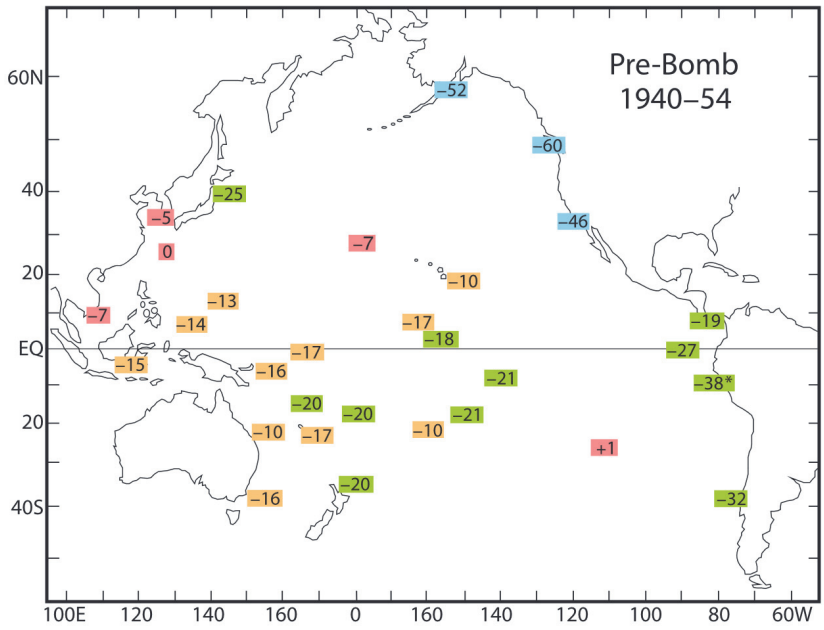

Figure 6. $\Delta^{14}C$ deficits in the Pacific during prebomb time (1940–1954). Okinawa reference = −41‰. The deficits with red backgrounds range from −7 to +1. Orange deficits range from −10 to −19. Green deficits range from −20 to −39. Blue deficits are larger than −40. The −38 deficit off Peru has an asterisk because the shells from which the deficit was derived were collected before 1940.

6. Deficit Maps for the Pacific Ocean

6.1. Prebomb Period (1940–1954)

Our prebomb map for the Pacific appears in Figure 6. Again, all the measurements used to make this map are from corals and shells. Okinawa, by definition, has a deficit of zero. Apart from Okinawa itself, the prebomb map has two small (red) deficits in the subtropical gyres, one from Kure Atoll (−7) at 28°N and one from Easter Island (+1) at 27°S. The area near Hawaii has a medium (orange) deficit of −10. Unlike the prebomb map for the Atlantic in Figure 3, the prebomb map for the Pacific has three extra large (blue) deficits along the coast of North America.

The area off Peru has a prebomb deficit of −38. This value comes from four shells that were collected off the coast of Peru in 1908 and 1926 and analyzed by Jones et al. (2009) (see page 12 of the supporting information). (The Peru deficit appears on the map with an asterisk because the four shells grew in the ocean before 1940). The measured deficit fits very well with the deficit expected from TDB91, −35 to −40. The Galapagos Islands to the north have a prebomb deficit of −27.

The most important deficits on the map are the large and medium deficits that stretch across the Pacific between 18°S (Fiji and Tahiti) and 13.5°N (Guam). The band covers an enormous area that stretches all the way across the Pacific. As in the Atlantic, the deficits shrink from east to west. They also grade lower from south of the equator to north of the equator, that is, from −21 and −20 at Tahiti, Fiji, and Vanuatu to −17, −14, and −13 at Palmyra, Palau, and Guam, respectively. As in the Atlantic, the deficits near the equator do not stand out against the deficits coming into the region from the east.

As mentioned above, the prebomb map also has three extra large deficits off Kodiak Island, Vancouver Island, and Southern California. These deficits are substantially larger than the deficits in the equatorial band. The surface waters in these areas are therefore presumed to have a deeper source than the water that is drawn up to the surface off Peru. The Pacific section of the supporting information (pages 13 and 14) shows that the low-$\Delta^{14}C$ water in all three areas seems to have been drawn up from the deep ocean initially near the Kamchatka Peninsula.

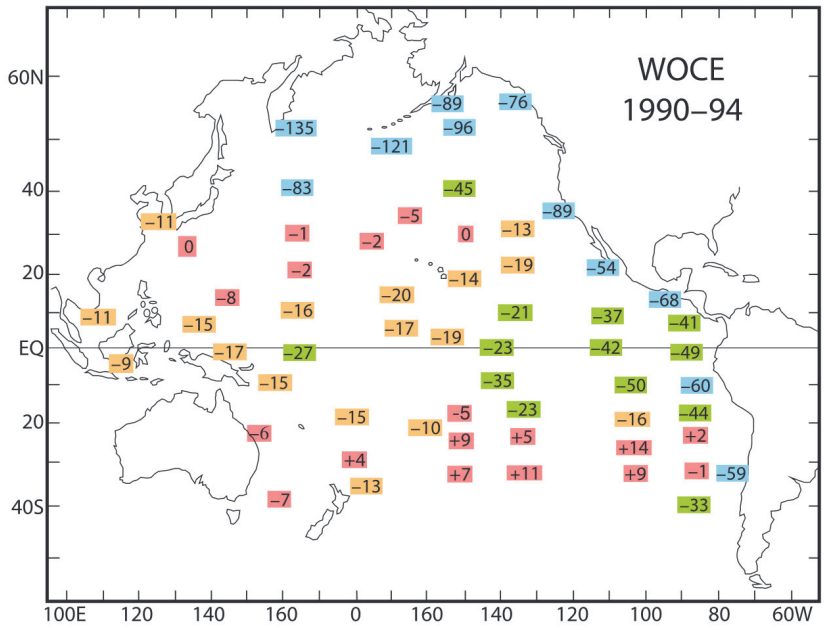

Figure 7. $\Delta^{14}C$ deficits in the Pacific during the World Ocean Circulation Experiment (WOCE) era (1990–1994). Okinawa reference = 116‰. The deficits with red backgrounds range from −8 to +14. Orange deficits range from −9 to −20. Green deficits range from −21 to −49. Blue deficits are larger than −50.

6.2. WOCE Era (1990–1994)

The WOCE map for the Pacific in Figure 7 is mostly based on seawater samples. The subtropical gyres were well sampled during this time period and provide a number of small (red) deficits for the map. The red deficits are notably positive in the South Pacific.

The medium (orange) deficits in the western half of the equatorial Pacific are similar to the deficits in the prebomb map. The large (green) deficits in the eastern Pacific, however, are larger. The Galapagos Islands, for example, have a deficit of −49 in Figure 7 compared to −27 in Figure 6. The Peru upwelling zone has a deficit of −60 compared with a prebomb deficit of −38. So, while the Peru-Galapagos difference remained about the same, the surface waters in both areas were 22‰ lower in $\Delta^{14}C$ during WOCE, in relation to Okinawa, than they were during prebomb time.

The larger WOCE deficits in the eastern Pacific are most likely due to the fact that the SAMW reaching Peru has a transit time of about 30 years (Rodgers et al., 2003). If so, the water upwelling off Peru in the early 1990s would have last been in contact with the atmosphere during the early years of the bomb era. As such, the water upwelling off Peru during WOCE would have had some bomb ^{14}C but not as much as the surface waters near Okinawa. This would account for the larger deficits during WOCE.

The area north of the Galapagos Islands in Figure 7 had a deficit during WOCE of −41. This value comes from five water samples collected between 2° and 9°N along ~88°W. Two of these samples were collected within the Costa Rica Dome (Wyrtki, 1964). The Dome samples would have a deficit of −53 by themselves, which is much larger than the deficit from the other three samples, −32. Kessler (2006) argues that the water drawn up to the surface in the Costa Rica Dome is closely related to the subantarctic water that is drawn up to the surface off Peru.

The map in Figure 7 has a number of extra large deficits in the subarctic zone. The largest by far is the −135 value from the area near the Kamchatka Peninsula. The Gulf of Alaska has a deficit of −96. These areas are located near the western and eastern centers of the North Pacific's subarctic gyre, respectively. The cyclonic circulation about the western gyre center, in particular, and the general divergence of the Ekman transport, seem to be drawing deep water directly up to the surface in this area from the deep North Pacific.

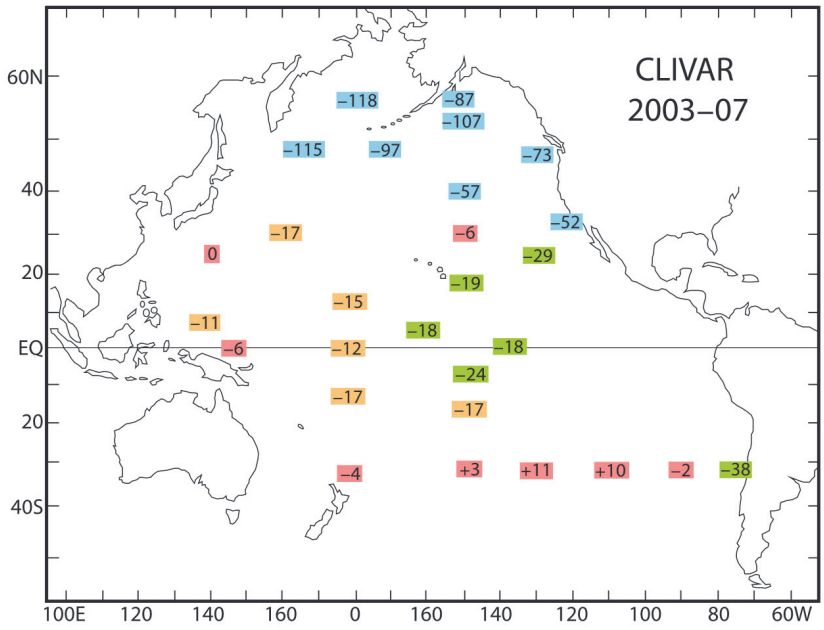

Figure 8. $\Delta^{14}C$ deficits in the Pacific during the CLIVAR era (2003–2007). Okinawa reference = 84‰. The deficits with red backgrounds range from −6 to +11. Orange deficits range from −10 to −17. Green deficits range from −18 to −39. Blue deficits are larger than −40.

6.3. CLIVAR Era (2003–2007)

Our CLIVAR map for the Pacific in Figure 8 has a number of extra large deficits in the North Pacific but is devoid of observations in the eastern tropical Pacific. A sequence of positive deficits along 32.5°S matches the sequence of WOCE deficits in this area. The deficits in the central and western sectors of the equatorial Pacific are smaller than the WOCE deficits in these areas, as one would expect from the changeover from the bomb era to the fossil fuel era.

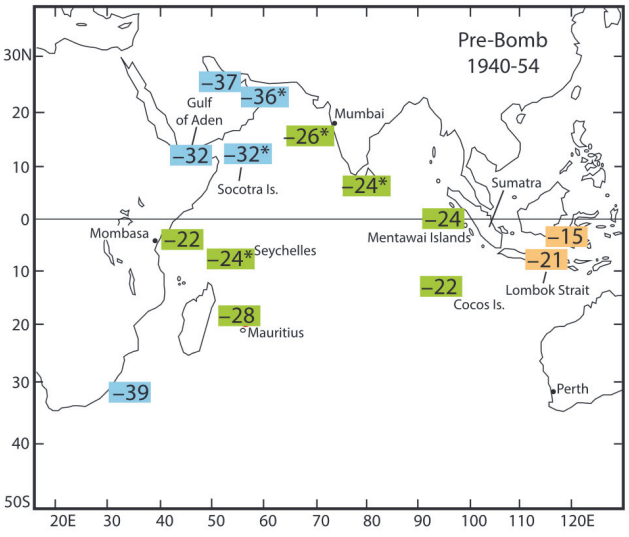

Figure 9. $\Delta^{14}C$ deficits in the Indian Ocean during the prebomb era (1940–1954). Okinawa reference = −41‰. Two orange deficits in the Indonesian seas have values of −15 and −21. All the prebomb deficits in the Indian Ocean are larger than −21. The green deficits range from −22 to −31. The blue deficits are larger than −32. The five deficits with asterisks are based on shell samples collected before 1940.

7. Deficit Maps for the Indian Ocean

Two maps have been constructed for the Indian Ocean, one for the prebomb period (Figure 9) and one for the WOCE era (Figure 10). The most striking feature of the two maps is a tendency toward large and extra large deficits. There are basically no small deficits anywhere in the Indian Ocean during either time period. Our color scale has been shifted to accommodate the larger values.

7.1. Prebomb Period

Our database for the Indian Ocean has prebomb observations from only eight locations. We have therefore added five observations from shells that were collected before 1940 and analyzed by Southon et al. (2002; see pages 18 and 19 in the supporting information). These values appear with asterisks on the prebomb map in Figure 9.

The northern Arabian Sea is a well-known upwelling area (Smith & Bottero, 1977) and our prebomb map has four deficits from this area. The four deficits range from −32 to −37 and are therefore similar in magnitude to the prebomb deficits off Northwest Africa and Peru.

The water drawn up to the surface in the Arabian Sea comes from a low-oxygen zone that extends from the base of the euphotic zone down to ~1,000 m (Morrison et al., 1999). Studies of the oxygen balance show

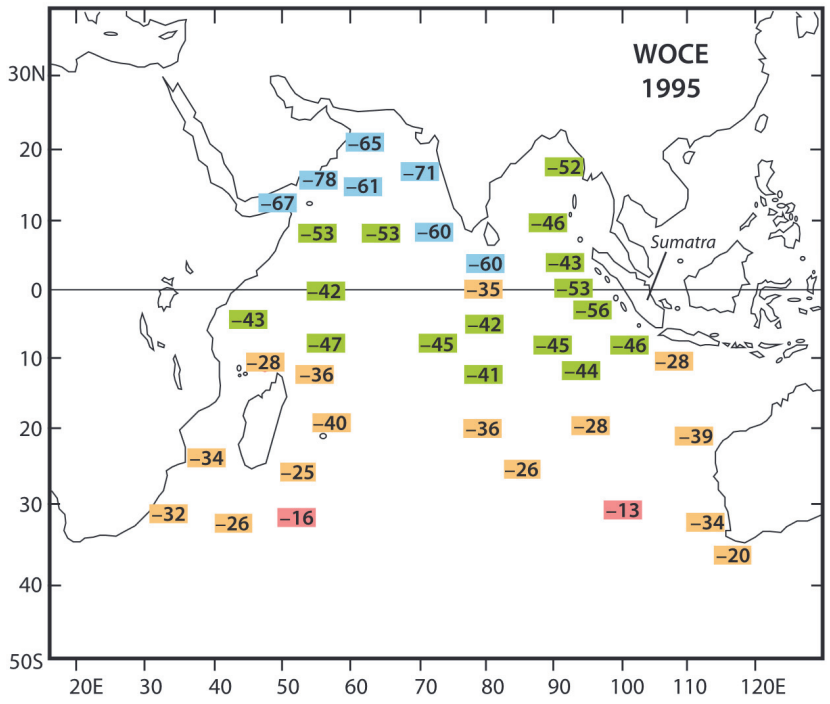

Figure 10. $\Delta^{14}C$ deficits in the Indian Ocean during the World Ocean Circulation Experiment (WOCE) era (1994–1996). Okinawa reference = 108‰. Two deficits along 30°S have values of −13 and −16. Orange deficits range from −20 to −39. Green deficits range from −40 to −59. The blue deficits in the Arabian Sea have values of −60 or larger.

that the input of oxygen comes mainly from an inflow of intermediate-depth water from the ACC (McCreary et al., 2013; Olson et al., 1993; Swallow, 1984). According to Swallow (1984), the upwelling in the Arabian Sea is the most likely "sink" for the inflow from the south.

Swallow (1984) describes the equatorial region as a "holding tank" in which the inflow from the south shifts off to the east under the Equatorial Counter Current and then back to the west in subsurface equatorial jets. The dissolved oxygen of the inflow is reduced during the diversion by the rain of organic matter from above and by mixing with older water below. As a result, the inflow from the south is fairly low in oxygen before it reaches the Arabian Sea.

The rest of the Indian Ocean has prebomb deficits between −22 and −28. The smallest deficit in this group is from Cocos atoll at 12°S, which lies along the path of the Indonesian Throughflow from the Pacific (Andrews, Asami, et al., 2016; Toggweiler & Trumbore, 1985). While the −22 deficit from Cocos atoll and the −21 deficit in Lombok Strait are similar, the rest of the prebomb deficits in this part of the Indian Ocean are larger. This suggests that the Throughflow is not the source of the large prebomb deficits in the Indian Ocean.

7.2. WOCE Era (1995)

The observations used to construct the WOCE map in Figure 10 are from samples collected between December 1994 and January 1996. The Okinawa reference value for this time period is 108‰. The smallest deficits have values of −13 and −16.

The WOCE map has six extra large deficits in the Arabian Sea. The largest, −78, is from the border area between Yemen and Oman. This area is near the core of the upwelling zone off Oman (Smith & Bottero, 1977). The next largest deficit, −71, is from an upwelling area off the west coast of India (Luis & Kawamura, 2004). The largest deficit outside of the Arabian Sea, −56, is offshore from a minor upwelling center off Central Sumatra at 4°S (Susanto et al., 2001). Overall, the WOCE map features a fairly continuous gradation from extra large deficits in the Arabian Sea to medium-sized deficits along 30°S.

The WOCE deficits in the Arabian Sea are notably larger than those in the prebomb map in Figure 9. As we did for the eastern Pacific, we would attribute the WOCE deficits to a transit time from the ACC to the upwelling zone in the Arabian Sea of 30 years or more. A long transit time would be consistent with the equatorial holding-tank idea in Swallow (1984).

The WOCE deficits between 10°S and 30°S are also substantially larger than the contemporary deficits in the western equatorial Pacific (Figure 7). This reinforces the view above that the Pacific water flowing through the Indonesian Seas is not the source of the deficits in the Indian Ocean. This leaves the Arabian Sea as the most likely source. It would appear that the upwelling in the Arabian Sea has a very large influence on the surface $\Delta^{14}C$ across the entire Indian Ocean (Southon et al., 2002).

8. Discussion

Three findings emerge from the observations above that lead to our three main conclusions. The first is that the largest ^{14}C deficits north of the ACC are associated with the upwelling zones along or near the ocean's margins. There are no conspicuous ^{14}C minima anywhere else. Thus, most of the upwelling north of the ACC would appear to be taking place in or near the upwelling zones along the margins.

The second finding is that the water reaching the surface in these areas had levels of $\Delta^{14}C$ before the bomb tests that seem to match the prebomb $\Delta^{14}C$ of the SAMW in the South Pacific. Thus, most of the water upwelling north of the ACC would seem to be mode or intermediate water from the ACC. The water upwelling off Kamchatka, in the Gulf of Alaska, and off California and Mexico would be exceptions in this regard.

The third finding is that the ^{14}C deficits from the upwelling areas seem to extend across the ocean basins. This implies that the spreading from the upwelling areas is fairly rapid, which implies, in turn, that the volumes of water drawn up to the surface in the upwelling areas per unit time are quite large—too large, it would seem, to be explained by the alongshore winds blowing over the upwelling zones themselves.

8.1. Rates of Upwelling and the Upwelling Mechanism

The upwelling along the ocean's margins is thought to be driven by winds that blow parallel to the coast. Detailed knowledge of the direction and strength of the wind can be used to estimate the volume of upwelling. Messié et al. (2009) have estimated the volumes of upwelling for four major upwelling systems. They found that 2 Sv is drawn up to the surface between 6°S and 16°S off Peru, 1.7 Sv is drawn up between 18° and 28°S off Namibia, 1.7 Sv is drawn between 12° and 22°N off Northwest Africa, and 1 Sv is drawn up between 34° and 44°N off California. Smith and Bottero (1977) estimated that 8 Sv is drawn up to the surface off Oman during July, August, and September. Eight Sv of upwelling over 3 months is equivalent to 2 Sv of upwelling over a full year.

These figures seem at odds with the results in our maps. It seems unlikely, for example, that 2 Sv of upwelling off Peru plus a smaller amount in the Costa Rica Dome (Wyrtki, 1964) could maintain ^{14}C deficits that extend across the entire equatorial Pacific. Our suspicion in this regard can be crudely quantified because the exchange of CO_2 between the ocean and atmosphere continually reduces the deficits generated by the upwelling. If one knows the gas exchange rates and the area over which they operate, one can estimate the volume of upwelling.

As shown in Figure 6, the water upwelling off Peru during prebomb time was 38‰ lower in $\Delta^{14}C$ than the surface waters at Okinawa. The surface waters between 18°S and 13.5°N in the equatorial band were about 19‰ lower on average. Thus, the gas exchange in the band seems to have reduced the initial deficit by half. We take this to mean that gas exchange and the upwelling had equal and opposite effects on the surface $\Delta^{14}C$.

A 50-m surface layer contains about 100 moles/m^2 of CO_2. The average gas exchange rate for the equatorial zone in Figure 6 is about 12 moles·m^{-2}·year^{-1} (as shown in Figure 3 in Toggweiler et al., 1989). This means that the CO_2 in the upper 50 m is turned over every 8.3 years by gas exchange (100 moles/m^2 ÷ 12 moles·m^{-2}·year^{-1} = 8.3 years). An upwelling of 6 m/year would be required to accomplish the same thing (50 m ÷ 6 m/year = 8.3 years). The low-$\Delta^{14}C$ waters of the equatorial Pacific cover about

55×10^{12} m^2. So ~10 Sv must be brought up from below to maintain the deficit against gas exchange (6 m/year $\times$ 55×10^{12} m^2 = 3.3×10^{14} m^3/year = 10.5 Sv).

In making this calculation we assume that the equatorial zone has no other sources of low-$\Delta^{14}C$ water besides the eastern margin. Following TDB91, we assume that the thermocline water upwelling along the equator is higher in $\Delta^{14}C$ and is therefore not a source of low-$\Delta^{14}C$ water. We implicitly include the upwelling in the Costa Rica Dome and along the Chilean margin in the eastern margin source.

Similar calculations can be made for the Atlantic and Indian Ocean. The area covered by low-$\Delta^{14}C$ water is not as great in the Atlantic, but the gas exchange rate is higher. As shown earlier, the entire Indian Ocean north of 30°S seems to be influenced by the low-$\Delta^{14}C$ water that is drawn up to the surface in the Arabian Sea.

An alternative approach is to simply consider the thickness of the SAMW-containing layer in the South Pacific and the time required to fill or drain this layer with SAMW. The SAMW layer is several hundred meters thick in the south and thins toward the equator. The fill/drain time would seem to be about 30 years, given that the SAMW off Peru had some bomb ^{14}C during WOCE. With a volume of ~11×10^{15} m^3 (i.e., 70×10^{12} m^2 $\times$ 150 m), the implied inflow/outflow is ~11.5 Sv, which is much closer to 10 Sv than to 2 Sv.

Similar amounts of throughput emerge from inverse box model studies. Lumpkin and Speer (2007) constructed an overturning stream function for the Atlantic from the transports across six zonal sections and the air-sea fluxes between the sections. They found that 16 Sv enters the Atlantic in the mode and intermediate water density class and is made into North Atlantic Deep Water (NADW) in the North Atlantic. They also found that ~10 Sv of the inflow is shifted up to the surface somewhere south of 24°N in the tropical Atlantic. (The remaining 6 Sv passes through the tropical Atlantic below the surface with minimal alteration.) Wunsch (1984) determined earlier that 7–10 Sv of low-$\Delta^{14}C$ water enters the tropical Atlantic from the south, upwells to the surface and then leaves the tropical Atlantic to the north.

Sloyan et al. (2003) have examined the upwelling of mode and intermediate waters in the Pacific with an inverse box model of the equatorial zone. They determined that 9 Sv of mode and intermediate water reaches the surface somewhere between 95°W and the American coast. In the Indian Ocean, Shi et al. (2002) have examined the transports across 9°N into and out of the Arabian Sea. They found a net inflow above 500 m (via the Somali Current) that balances 9.5 Sv of upwelling to the north of the section.

The inverse models and the surface $\Delta^{14}C$ are therefore in broad agreement in regard to the volumes of upwelling: ~10 Sv of mode and intermediate water from the ACC seem to be reaching the surface in each ocean basin in the tropics. The two approaches point in different directions, however, in regard to the mechanism.

The inverse models call upon diapycnal mixing to explain the upwelling. Large amounts of diapycnal mixing are called upon, in particular, to transform the relatively dense inflows from the ACC into lighter water (Lumpkin & Speer, 2003; Sloyan et al., 2003). Once transformed, the lighter water can, in theory, be displaced up to the surface by the denser water flowing in.

The surface $\Delta^{14}C$, on the other hand, suggests that much of the upwelling occurs along the margins in areas where the mode and intermediate waters are drawn directly up to the surface. The water upwelling in these areas can be transformed by air-sea fluxes. So, if all the upwelling is indeed taking place in areas like these, the need for diapycnal mixing is greatly reduced. But some other mechanism is then needed to account for the volumes of upwelling.

It is important to emphasize that our observations are quite sparse and do not provide an unambiguous mapping of the upwelling areas and the intensity of the upwelling. The upwelling in the real ocean could be dispersed away from the margins in a way that would limit the role of air-sea fluxes in the transformation of the mode and intermediate waters from the ACC.

8.2. Two Kinds of Upwelling

Given all the information above, it would seem that there are two kinds of upwelling at work in or near the upwelling zones. One is a response to the winds in the upwelling zones themselves. The other is associated with the overturning of NADW. (SAMW reaching the surface in the upwelling zones is a clear sign of the latter.)

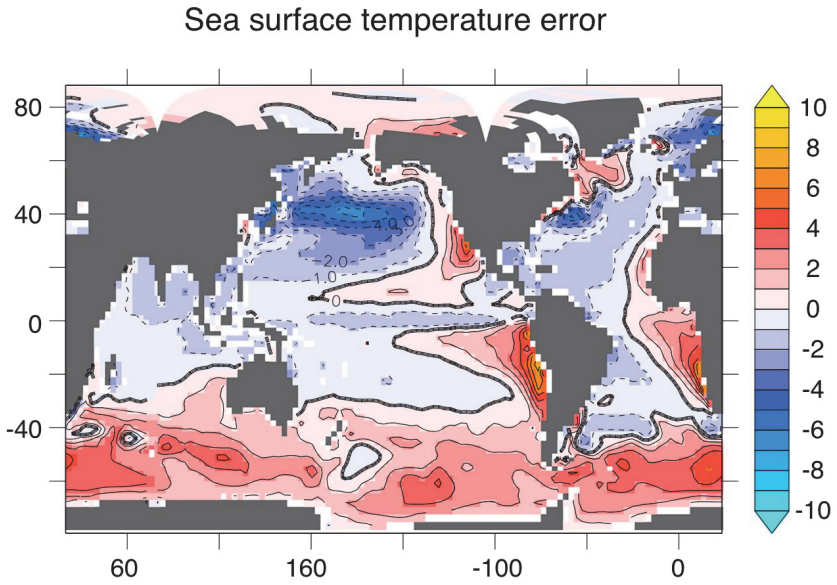

Figure 11. Sea surface temperature errors in the coupled model in Galbraith et al. (2011). Areas with large positive sea surface temperature errors in the model coincide with the areas with large $\Delta^{14}C$ deficits in Figures 4 and 7.

The volumes of upwelling associated with the second type of upwelling are much larger than the volumes of upwelling associated with the first. As a result, there is a great deal of "extra upwelling" in or near the upwelling zones, that is, more upwelling than expected from the local winds. The extra upwelling accounts for the extensive spreading of the low-$\Delta^{14}C$ water in our maps.

In our companion paper, we simulate the surface $\Delta^{14}C$ in two low-resolution ocean general circulation models. Interestingly, the extra upwelling does not develop in either model. As might be expected, the missing upwelling is reflected in other properties. Figure 11 is a map of the departure of the simulated sea surface temperatures (SSTs) from the observed SSTs in one of the models. Not enough cool water is drawn up to the surface and the simulated SSTs offshore from the upwelling areas are too warm. Overly warm SSTs in these areas are a common deficiency in climate-scale coupled models (Wang et al., 2014). So what are the models missing? What accounts for the extra upwelling?

Model studies by Lu et al. (1998) and McCreary et al. (2002) have tried to plug this gap. The models in question are limited to the Pacific basin and are not general circulation models (GCMs) in the usual sense. Ten sverdrups of relatively dense subantarctic water are added to the model domains in the south and 10 Sv of light near-surface water are removed in the vicinity of the Indonesian Seas. The water removed via the Indonesian Seas is assumed to end up in the North Atlantic. The McCreary et al. model also shows how the subantarctic inflow is transformed off Costa Rica and Peru into the near-surface outflow.

The "extra upwelling" is put into the Lu et al. and McCreary et al. models via the imposed inflows and outflows (and the fact that the outflow has a lower density). But imposed inflows and outflows do not fully explain what the extra upwelling actually is and what typical GCMs are doing wrong.

We argue in the companion paper that the extra upwelling develops when the warm buoyant water in the western tropics is drawn away to the North Atlantic. Typical GCMs fail to produce the extra upwelling because very little of the warm buoyant water in the western tropics is drawn away.

9. Conclusions

The overturning of NADW is defined these days in terms of upwelling in the Southern Ocean and the formation of deep water in the North Atlantic (Marshall & Speer, 2012). The radioactive isotope ^{14}C is used here to show that the deep water upwelled in the Southern Ocean is upwelled to the surface again in the ocean basins to the north of the ACC. Most of the upwelling is found to take place in well-known upwelling

areas around the margins of the ocean basins. The big surprise is the volumes of upwelling, which are more commensurate with the ocean's large-scale overturning than the Ekman divergence in the upwelling areas themselves. Something similar is seen in the North Pacific, where deep water with a very low $\Delta^{14}C$ is drawn up to the surface in the western part of the subarctic gyre. This water becomes incorporated into the California Current and is upwelled again off Southern California and Mexico in a second stage that is analogous to the second upwelling seen in the tropics.

Inverse box models of the ocean's overturning circulation also find large volumes of upwelling in the same general areas but they call upon diapycnal processes to transform the relatively dense water below into the lighter water found near the surface (Lumpkin & Speer, 2003; Sloyan et al., 2003). We would argue that these transformations take place instead near the ocean's margins, and that the transformations occur mainly at the surface via air-sea fluxes. Shifting the upwelling toward the margins diminishes the need for diapycnal processes but begs the question—what sort of process can account for the volumes of upwelling? There must be an aspect of the ocean's large-scale circulation in which large volumes of subantarctic water flow into the upwelling zones and are then drawn away.

Acknowledgments

This study is based on hundreds of $\Delta^{14}C$ measurements made by other investigators. The authors would first like to acknowledge the important contributions made by the people who produced the measurements. The documentation for these contributions is given in the Supporting Information S1. The seawater measurements used in this study were made primarily at the National Ocean Sciences Accelerator Mass Spectrometry Facility (NOSAMS) at the Woods Hole Oceanographic Institution, and the authors would especially like to acknowledge Ann McNichol and Al Gagnon at NOSAMS for their contributions. Funding for this portion of the project was provided by U.S. National Science Foundation, through its support for NOSAMS and through numerous grants to R. M. K. and Ann McNichol during the WOCE, CLIVAR, and GO-SHIPS programs. E. R. M. D. would like to acknowledge support from the NSF Divison of Ocean Sciences (OCE-0551940, OCE-1458941, and OCE-0961980). R. M. K. would also like to acknowledge support from NSF Division of Ocean Sciences grants OCE-0825163, OCE-1155983, OCE-1558740, and their predecessors. The authors would also like to thank Harold Hudson who collected the coral head that was used to reconstruct the $\Delta^{14}C$ for the Florida Keys during the WOCE and CLIVAR eras. Reviews by John Dunne, Rong Zhang, Andrew Shao, Jorge Sarmiento, and two anonymous reviewers greatly improved the paper. Jeff Varanyak, Cathy Raphael, and Brendan Carter provided help with the figures. Gail Haller helped with the references.

References

Andrews, A. H., Asami, R., Iryu, Y., Kobayashi, D. R., & Camacho, F. (2016). Bomb-produced radio-carbon in the western tropical Pacific—Guam coral reveals operation-specific signals from the Pacific proving grounds. *Journal of Geophysical Research: Oceans*, *121*, 6351–6366. https://doi.org/10.1002/2016JC012043

Broecker, W. S., & Peng, T.-H. (1974). Gas exchange rates between air and sea. *Tellus*, *26*, 21–35.

Broecker, W. S., & Peng, T.-H. (1982). *Tracers in the Sea*, (p. 690). Palisades, NY: Lamont-Doherty Earth Observatory, Columbia University.

Broecker, W. S., Peng, T.-H., Ostlund, H. G., & Stuiver, M. (1985). The distribution of bomb radiocarbon in the ocean. *Journal of Geophysical Research*, *90*(C4), 6953–6970. https://doi.org/10.1029/JC090iC04p06953

Chavez, F. P., & Messié, M. (2009). A comparison of eastern boundary upwelling ecosystems. *Progress in Oceanography*, *83*(1-4), 80–96. https://doi.org/10.1016/j.pocean.2009.07.032

Dewar, G., Reimer, P. J., Sealy, J., & Woodborne, S. (2012). Holocene marine radiocarbon reservoir correction (ΔR) for the west coast of South Africa. *Holocene*, *22*(12), 1481–1489. https://doi.org/10.1177/0959683612449755

Druffel, E. M. (1981). Radiocarbon in annual coral rings from the eastern tropical Pacific Ocean. *Geophysical Research Letters*, *8*(1), 59–62. https://doi.org/10.1029/GL008i001p00059

Druffel, E. M., & Linick, T. W. (1978). Radiocarbon in annual coral rings of Florida. *Geophysical Research Letters*, *5*(11), 913–916. https://doi.org/10.1029/GL005i011p00913

Druffel, E. R. M. (1989). Decade time scale variability of ventilation in the North Atlantic: High precision measurements of bomb radiocarbon in banded corals. *Journal of Geophysical Research*, *94*(C3), 3271–3285. https://doi.org/10.1029/JC094iC03p03271

Druffel, E. R. M., Beaupre, S., Griffin, S., & Hwang, J. (2010). Variability of dissolved inorganic radiocarbon at a surface site in the Northeast Pacific Ocean. *Radiocarbon*, *52*(3), 1150–1157. https://doi.org/10.1017/S0033822200046221

Eiríksson, J., Knudsen, K. L., Larsen, G., Olsen, J., Heinemeier, J., Bartels-Jónsdóttir, H. B., et al. (2011). Coupling of palaeoceanographic shifts and changes in marine reservoir ages off North Iceland through the last millennium. *Palaeogeography, Palaeoclimatology, Palaeoecology*, *302*(1-2), 95–108. https://doi.org/10.1016/j.palaeo.2010.06.002

Galbraith, E. D., Kwon, E. Y., Gnanadesikan, A., Rodgers, K. B., Griffies, S. M., Bianchi, D., et al. (2011). Climate variability and radiocarbon in the CM2Mc Earth system model. *Journal of Climate*, *24*(16), 4230–4254. https://doi.org/10.1175/2011JCLI3919.1

Goodkin, N. F., Druffel, E. R. M., Hughen, K. A., & Doney, S. C. (2012). Two centuries of limited variability in subtropical North Atlantic thermocline ventilation. *Nature Communications*, *3*(1), 803. https://doi.org/10.1038/ncomms1811

Håkansson, S. (2010). A reservoir age for the coastal waters of Iceland. *Geologiska Föreningens I Stockholm Förhandlinge*, *105*(1), 64–67. https://doi.org/10.1080/11035898309455300

Hardman-Mountford, N. J., Richardson, A. J., Agenbag, J. J., Hagen, E., Nykjaer, L., Shillington, F. A., & Villacastin, C. (2003). Ocean climate of the south east Atlantic observed from satellite data and wind models. *Progress in Oceanography*, *59*(2-3), 181–221. https://doi.org/10.1016/j.pocean.2003.10.001

Iudicone, D., Speich, S., Madec, G., & Blanke, B. (2008). The global conveyor from a Southern Ocean perspective. *Journal of Physical Oceanography*, *38*(7), 1401–1425. https://doi.org/10.1175/2007JPO3525.1

Jones, K. B., Hodgins, G. W. L., Etayo-Cadavied, M. F., & Andrus, C. F. T. (2009). Upwelling signals in radiocarbon from early 20th-century Peruvian bay scallop (Argopecten purpuratus) shells. *Quaternary Research*, *72*(3), 452–456. https://doi.org/10.1016/j.yqres.2009.07.008

Jónsson, S., & Valdimarsson, H. (2012). Water mass transport variability to the north Icelandic shelf, 1994–2010. *ICES Journal of Marine Science*. https://doi.org/10.1093/icejms/fss024

Kessler, W. S. (2006). The circulation of the eastern tropical Pacific: A review. *Progress in Oceanography*, *69*(2-4), 181–217. https://doi.org/10.1016/j.pocean.2006.03.009

Kilbourne, K. H., Quinn, T. M., Guilderson, T. P., Webb, R. S., & Taylor, F. W. (2007). Decadal- to interannual-scale source water variations in the Caribbean Sea recorded by Puerto Rican coral radiocarbon. *Climate Dynamics*, *29*(1), 51–62. https://doi.org/10.1007/s00382-007-0224-2

Knudsen, K. L., Eiríksson, J., Jansen, E., Jiang, J., Rytter, F., & Gudmundsdóttir, E. R. (2004). Palaeoceanographic changes off North Iceland through the last 1200 years. *Quaternary Science Reviews*, *23*(20-22), 2231–2246. https://doi.org/10.1016/j.quascirev.2004.08.012

Lu, P., McCreary, J. P., & Klinger, B. A. (1998). Meridional circulation cells and the source waters of the equatorial undercurrent. *Journal of Physical Oceanography*, *28*(1), 62–84. https://doi.org/10.1175/1520-0485(1998)028<0062:MCCATS>2.0.CO;2

Luis, A. J., & Kawamura, H. (2004). Air-sea interaction, coastal circulation, and primary production in the eastern Arabian Sea: A review. *Journal of Oceanography*, *60*(2), 205–218. https://doi.org/10.1023/B:JOCE.0000038327.33559.34

Lumpkin, R., & Speer, K. (2003). Large-scale vertical and horizontal circulation in the North Atlantic Ocean. *Journal of Physical Oceanography*, *33*(9), 1902–1920. https://doi.org/10.1175/1520-0485(2003)033<1902:LVAHCI>2.0.CO;2

Lumpkin, R., & Speer, K. (2007). Global Ocean meridional overturning. *Journal of Physical Oceanography*, *37*(10), 2550–2562. https://doi.org/10.1175/JPO3130.1

Marshall, J., & Speer, K. (2012). Closure of the meridional overturning circulation through Southern Ocean upwelling. *Nature Geoscience*, *5*(3), 171–180. https://doi.org/10.1038/ngeo1391

Massé, G., Rowland, S. J., Sicre, M.-A., Jacob, J., Jansen, E., & Belt, S. T. (2008). Abrupt climate changes for Iceland during the last millennium: Evidence from high-resolution sea-ice reconstructions. *Earth and Planetary Science Letters*, *269*(3-4), 565–569. https://doi.org/10.1016/j.epsl.2008.03.017

McCreary, J. P., Yu, Z., Hood, R. R., Vinaychandran, P. N., Furue, R., Ishida, A., & Richards, K. J. (2013). Dynamics of the Indian-Ocean oxygen minimum zones. *Progress in Oceanography*, *112-113*, 15–37. https://doi.org/10.1016/j.pocean.2013.03.002

McCreary, J. P., Lu, P., & Yu, Z. (2002). Dynamics of Pacific subsurface countercurrents. *Journal of Physical Oceanography*, *32*(8), 2379–2404. https://doi.org/10.1175/1520-0485(2002)032<2379:DOTPSC>2.0.CO;2

McDuffee, K., & Druffel, E. R. M. (2007). Daily variability of dissolved inorganic radiocarbon in Sargasso Sea surface water. *Marine Chemistry*, *106*(3-4), 510–515. https://doi.org/10.1016/j.marchem.2007.05.003

Messié, M., Ledesma, J., Kolber, D. D., Michisaki, R. P., Foley, D. G., & Chavez, F. P. (2009). Potential new production estimates in four eastern boundary upwelling ecosystems. *Progress in Oceanography*, *83*(1-4), 151–158. https://doi.org/10.1016/j.pocean.2009.07.018

Mittelstaedt, E. (1983). The upwelling area off northwest Africa—A description of phenomena related to coastal upwelling. *Progress in Oceanography*, *12*(3), 307–331. https://doi.org/10.1016/0079-6611(83)90012-5

Morrison, J. M., Codispoti, L. A., Smith, S. L., Wishner, K., Flagg, C., Gardner, W. D., et al. (1999). The oxygen minimum zone in the Arabian Sea in 1995. *Deep-Sea Research Part II: Topical Studies in Oceanography*, *46*(8-9), 1903–1931. https://doi.org/10.1016/S0967-0645(99)00048-X

Ndeye, M. (2008). Marine reservoir ages in northern Senegal and Mauritania coastal waters. *Radiocarbon*, *50*(2), 281–288. https://doi.org/10.1017/S0033822200033580

Nelson, G., & Hutchings, L. (1983). The Benguela upwelling area. *Progress in Oceanography*, *12*(3), 333–356. https://doi.org/10.1016/0079-6611(83)90013-7

Olson, D. B., Hitchcock, G. L., Fine, R. A., & Warren, B. A. (1993). Maintenance of the low-oxygen layer in the central Arabian Sea. *Deep-Sea Research Part II: Topical Studies in Oceanography*, *40*(3), 673–685. https://doi.org/10.1016/0967-0645(93)90051-N

Pastor, M. V., Peña-Izquiderdo, J., Pelegri, J. L., & Marrero-Díaz, Á. (2012). Meridional changes in water mass distributions off NW Africa during November 2007/2008. *Ciencias Marinas*, *38*(1B), 223–244.

Rodgers, K. B., Blanke, B., Madec, G., Aumont, O., Ciais, P., & Dutay, J.-C. (2003). Extratropical sources of equatorial Pacific upwelling in an OGCM. *Geophysical Research Letters*, *30*(2), 1084. https://doi.org/10.1029/2002GL016003

Scourse, J. D., Wanamaker, A. D., Weidman, C., Heinemeier, J., Reimer, P. J., Butler, P. G., et al. (2012). The marine radiocarbon bomb pulse across the temperate North Atlantic: A compilation of $\Delta^{14}C$ time histories from *Arctica islandica* growth increments. *Radiocarbon*, *54*(2), 165–186. https://doi.org/10.2458/azu_js_rc.v54i2.16026

Shi, W., Morrison, J. M., & Bryden, H. L. (2002). Water, heat and freshwater flux out of the northern Indian Ocean in September-October 1995. *Deep Sea Research Part II: Topical Studies in Oceanography*, *49*(7-8), 1231–1252. https://doi.org/10.1016/S0967-0645(01)00154-0

Sloyan, B. M., Johnson, G. C., & Kessler, W. S. (2003). The Pacific cold tongue, a pathway for inter-hemispheric exchange. *Journal of Physical Oceanography*, *33*(5), 1027–1043. https://doi.org/10.1175/1520-0485(2003)033<1027:TPCTAP>2.0.CO;2

Sloyan, B. M., & Rintoul, S. R. (2001). Circulation, renewal, and modification of Antarctic mode and intermediate water. *Journal of Physical Oceanography*, *31*(4), 1005–1030. https://doi.org/10.1175/1520-0485(2001)031<1005:CRAMOA>2.0.CO;2

Sloyan, B. M., Talley, L. D., Chereskin, T. K., Fine, R., & Holte, J. (2010). Antarctic intermediate water and Subantarctic mode water formation in the southeast Pacific: The role of turbulent mixing. *Journal of Physical Oceanography*, *40*(7), 1558–1574. https://doi.org/10.1175/2010JPO4114.1

Smith, R. L., & Bottero, J. S. (1977). On upwelling in the Arabian Sea. In M. Angel (Ed.), *A Voyage of Discovery*, (pp. 291–304). Oxford: Pergamon Press.

Southon, J., Kashgarian, M., Fontugne, M., Metivier, B., & Yim, W. W.-S. (2002). Marine reservoir corrections for the Indian Ocean and Southeast Asia. *Radiocarbon*, *44*(1), 167–180. https://doi.org/10.1017/S0033822200064778

Speer, K., Rintoul, S. R., & Sloyan, B. (2000). The diabatic deacon cell. *Journal of Physical Oceanography*, *30*(12), 3212–3222. https://doi.org/10.1175/1520-0485(2000)030<3212:TDDC>2.0.CO;2

Stuiver, M., & Polach, H. A. (1977). Reporting of ^{14}C data. *Radiocarbon*, *19*(3), 355–363. https://doi.org/10.1017/S0033822200003672

Susanto, R. D., Gordon, A. L., & Zheng, Q. (2001). Upwelling along the coasts of Java and Sumatra and its relation to ENSO. *Geophysical Research Letters*, *28*(8), 1599–1602. https://doi.org/10.1029/2000GL011844

Swallow, J. C. (1984). Some aspects of the physical oceanography of the Indian Ocean. *Deep Sea Research Part A. Oceanographic Research Papers*, *31*(6–8), 639–650. https://doi.org/10.1016/0198-0149(84)90032-3

Talley, L. D. (2008). Freshwater transport estimates and the global overturning circulation: Shallow, deep and throughflow components. *Progress in Oceanography*, *78*(4), 257–303. https://doi.org/10.1016/j.pocean.2008.05.001

Tanaka, N., Monaghan, M. C., & Turekian, K. K. (1990). ^{14}C balance for the Gulf of Maine, Long Island sound, and the northern middle Atlantic bight: Evidence for the extent of Antarctic intermediate water contribution. *Journal of Marine Research*, *48*(1), 75–87. https://doi.org/10.1357/002224090784984641

Toggweiler, J. R., Dixon, K., & Broecker, W. (1991). The Peru upwelling and the ventilation of the South Pacific thermocline. *Journal of Geophysical Research*, *96*(C11), 20,467–20,497. https://doi.org/10.1029/91JC02063

Toggweiler, J. R., Dixon, K., & Bryan, K. (1989). Simulations of radiocarbon in a coarse-resolution World Ocean model, 1, steady state prebomb distributions. *Journal of Geophysical Research*, *94*(C6), 8217–8242. https://doi.org/10.1029/JC094iC06p08217

Toggweiler, J. R., Druffel, E. R. M., Key, R. M., & Galbraith, E. D. (2019). Upwelling in the ocean basins north of the ACC: 2. How cool subantarctic water reaches the surface in the tropics. *Journal of Geophysical Research: Oceans*, *124*, 2609–2625. https://doi.org/10.1029/2018JC014795

Toggweiler, J. R., & Samuels, B. (1993). New radiocarbon constraints on the upwelling of abyssal water to the ocean's surface. In M. Heimann (Ed.), *The Global Carbon Cycle*, *NATO ASI Series*, (Vol. 1-15, pp. 333–366). Berlin: Springer.

Toggweiler, J. R., & Trumbore, S. (1985). Bomb-test ^{90}Sr in Pacific and Indian Ocean surface water as recorded by banded corals. *Earth and Planetary Science Letters*, *74*(4), 306–314. https://doi.org/10.1016/S0012-821X(85)80002-9

Wang, C., Zhang, L., Lee, S.-K., Wu, L., & Mechoso, C. R. (2014). A global perspective on CMIP5 model biases. *Nature Climate Change*, *4*(3), 201–205. https://doi.org/10.1038/nclimate2118

Wunsch, C. (1984). An estimate of the upwelling rate in the equatorial Atlantic based on the distribution of bomb radiocarbon and quasi-geostrophic dynamics. *Journal of Geophysical Research*, *89*(C5), 7971–7978. https://doi.org/10.1029/JC089iC05p07971

Wyrtki, K. (1964). Upwelling in the Costa Rica dome. *Fishery Bulletin*, *63*(2), 355–372.

References From the Supporting Information

Andrews, A. H., Siciliano, D., Potts, D. C., DeMartini, E. E., & Covarrubias, S. (2016). Bomb radio-carbon and the Hawaiian archipelago: Coral, otoliths, and seawater. *Radiocarbon*, *58*(3), 531–548. https://doi.org/10.1017/RDC.2016.32

Angulo, R. J., de Souza, M. C., Reimer, P. J., & Sasaoka, S. K. (2005). Reservoir effect of the southern and southeastern Brazilian coast. *Radiocarbon*, *47*(1), 67–73. https://doi.org/10.1017/S0033822200052206

Beck, J. W., Hewitt, L., Burr, G. S., Loret, J., & Hochstetter, F. T. (2003). Mata Ki Te Rangi: Eyes towards the heavens in Easter Island. In J. Loret, & J. T. Tanacredi (Eds.), *Easter Island*, (pp. 93–111). New York: Kluwever Academic/Plenum Publishers.

Bhushan, R., Somayajulu, B. L. K., Chakraborty, S., & Krishnaswami, S. (2000). Radiocarbon in the Arabian Sea water column: Temporal variations in bomb ^{14}C inventory since GEOSECS and CO_2 air-sea exchange rates. *Journal of Geophysical Research*, *105*(C6), 14,273–14,282. https://doi.org/10.1029/2000JC000255

Bien, G. S., Rakestraw, N. W., & Suess, H. E. (1960). Radiocarbon concentration in Pacific Ocean water. *Tellus*, *12*, 436–443.

Broecker, W. S., & Gerard, R. (1969). Natural radiocarbon in the Mediterranean Sea. *Limnology and Oceanography*, *14*(6), 883–888. https://doi.org/10.4319/lo.1969.14.6.0883

Broecker, W. S., & Olson, E. A. (1961). Lamont radiocarbon measurements VIII. *Radiocarbon*, *3*, 176–204. https://doi.org/10.1017/S0033822200020920

Burr, G. S., Beck, J. W., Correge, T., Cabioch, G., Taylor, F. W., & Donahue, D. J. (2009). Modern and Pleistocene reservoir ages inferred from South Pacific corals. *Radiocarbon*, *51*(1), 319–335. https://doi.org/10.1017/S0033822200033853

Burr, G. S., Beck, J. W., Taylor, F. W., Récy, J., Edwards, R. L., Cabioch, G., et al. (1998). A high-resolution radiocarbon calibration between 11,700 and 12,400 calendar years BP derived from ^{230}Th ages of corals from Espiritu Santo Island, Vanuatu. *Radiocarbon*, *40*(3), 1093–1105. https://doi.org/10.1017/S0033822200019147

Csanady, G. T., & Hamilton, P. (1988). Circulation of slopewater. *Continental Shelf Research*, *8*(5-7), 565–624. https://doi.org/10.1016/0278-4343(88)90068-4

Druffel, E. M. (1980). Radiocarbon in annual coral rings of Florida and Belize. *Radiocarbon*, *22*(2), 363–371. https://doi.org/10.1017/S0033822200009656

Druffel, E. R. M. (1987). Bomb radiocarbon in the Pacific: Annual and seasonal timescale variations. *Journal of Marine Research*, *45*(3), 667–698. https://doi.org/10.1357/002224087788326876

Druffel, E. R. M. (1996). Post-bomb radiocarbon records from surface corals of the tropical Atlantic Ocean. *Radiocarbon*, *38*(3), 563–572. https://doi.org/10.1017/S0033822200030095

Druffel, E. R. M. (1997). Pulses of rapid ventilation in the North Atlantic surface ocean during the past century. *Science*, *275*(5305), 1454–1457. https://doi.org/10.1126/science.275.5305.1454

Druffel, E. R. M., Bauer, J. E., & Griffin, S. (2005). Input of particulate organic and dissolved organic carbon from the Amazon to the Atlantic Ocean. *Geochemistry, Geophysics, Geosystems*, *6*, Q03009. https://doi.org/10.1029/2004GC000842

Druffel, E. R. M., & Griffin, S. (1995). Regional variability of surface ocean radiocarbon from southern Great Barrier Reef corals. *Radiocarbon*, *37*(2), 517–524. https://doi.org/10.1017/S0033822200031003

Druffel, E. R. M., & Griffin, S. (1999). Variability of surface ocean radiocarbon and stable isotopes in the southwestern Pacific. *Journal of Geophysical Research*, *104*(C10), 23,607–23,613. https://doi.org/10.1029/1999JC900212

Druffel, E. R. M., Griffin, S., Beaupre, S. R., & Dunbar, R. B. (2007). Oceanic climate and circulation changes during the past four centuries from radiocarbon in corals. *Geophysical Research Letters*, *34*, L09601. https://doi.org/10.1029/2006GL028681

Druffel, E. R. M., Griffin, S., Glynn, D. S., Dunbar, R. B., Mucciarone, D. A., & Toggweiler, J. R. (2014). Seasonal radiocarbon and oxygen isotopes in a Galapagos coral: Calibration with climate indices. *Geophysical Research Letters*, *41*, 5099–5105. https://doi.org/10.1002/2014GL060504

Druffel, E. R. M., Griffin, S., Guilderson, T. P., Kashgarian, M., Southon, J., & Schrag, D. P. (2001). Changes of subtropical North Pacific radiocarbon and correlation with climate variability. *Radiocarbon*, *43*(1), 15–25. https://doi.org/10.1017/S0033822200031593

Druffel-Rodriguez, K. C., Vetter, D., Griffin, S., Druffel, E. R. M., Dunbar, R. B., Mucciarone, D. A., et al. (2012). Radiocarbon and stable isotopes in Palmyra corals during the past century. *Geochimica et Cosmochimica Acta*, *82*, 154–162. https://doi.org/10.1016/j.gca.2010.11.028

Eastoe, C. J., Fish, S., Fish, P., Dulce Gaspa, M., & Long, A. (2002). Reservoir corrections for marine samples from the South Atlantic coast, Santa Catarina state, Brazil. *Radiocarbon*, *44*(1), 145–148. https://doi.org/10.1017/S0033822200064742

Fallon, S. J., & Guilderson, T. P. (2008). Surface water processes in the Indonesian throughflow as documented by a high-resolution coral $\Delta^{14}C$ record. *Journal of Geophysical Research*, *113*, C09001. https://doi.org/10.1029/2008JC004722

Gill, E. D. (1983). Australian sea levels in the last 15000 years—Victoria, S.E. Australia. In *Australian sea levels in the last 15 000 years: A review*, *Monograph Series*, (pp. 59–63). Townsville: James Cook University.

Gillespie, R. (1977). Sydney University natural radiocarbon measurements IV. *Radiocarbon*, *19*(1), 101–110. https://doi.org/10.1017/S0033822200003374

Gillespie, R., & Polach, H. A. (1979). The suitability of marine shells for radiocarbon dating of Australian prehistory. In R. Berger, & H. E. Suess (Eds.), *Radiocarbon Dating: Proceedings 9th International ^{14}C Conference*, (pp. 404–421). Berkeley: University of California Press.

Glynn, D., Druffel, E., Griffin, S., Dunbar, R., Osborne, M., & Sanchez-Cabeza, J. A. (2013). Early bomb radiocarbon detected in Palau archipelago corals. *Radiocarbon*, *55*(3), 1659–1664. https://doi.org/10.1017/S0033822200048578

Gordon, A. L. (1986). Interocean exchange of thermocline water. *Journal of Geophysical Research*, *91*(C4), 5037–5046. https://doi.org/10.1029/JC091iC04p05037

Gordon, A. L., Bosley, K. T., & Aikman, F. (1995). Tropical Atlantic water within the Benguela upwelling system at 27°S. *Deep Sea Research Part I: Oceanographic Research Papers*, *42*(1), 1–12. https://doi.org/10.1016/0967-0637(94)00032-N

Gordon, A. L., Susanto, R. D., Ffield, A., Huber, B. A., Pranowo, W., & Wirasantosa, S. (2008). Makassar Strait throughflow, 2004–2006. *Geophysical Research Letters*, *35*, L24605. https://doi.org/10.1029/2008GL036372

Grumet, N. S., Abram, N. J., Beck, J. W., Dunbar, R. B., Gagan, M. K., Guilderson, T. P., et al. (2004). Coral radiocarbon records of Indian Ocean water mass mixing and wind-induced upwelling along the coast of Sumatra, Indonesia. *Journal of Geophysical Research*, *109*, C05003. https://doi.org/10.1029/2003JC002087

Grumet, N. S., Guilderson, T. P., & Dunbar, R. B. (2002). Pre-bomb radiocarbon variability inferred from a Kenyan coral record. *Radiocarbon*, *44*(2), 581–590. https://doi.org/10.1017/S0033822200031933

Guilderson, T. P., Cole, J. E., & Southon, J. R. (2005). Pre-bomb $\Delta^{14}C$ variability and the Suess effect in Cariaco basin surface waters as recorded in hermatypic corals. *Radiocarbon*, *47*(1), 57–65. https://doi.org/10.1017/S003382220005219X

Guilderson, T. P., Fallon, S., Moore, M. D., Schrag, D. P., & Charles, C. D. (2009). Seasonally resolved surface water $\Delta^{14}C$ variability in the Lombok Strait: A coralline perspective. *Journal of Geophysical Research*, *114*, C07029. https://doi.org/10.1029/2008JC004876

Guilderson, T. P., Schrag, D. P., & Cane, M. A. (2004). Surface water mixing in the Solomon Sea as documented by a high-resolution coral ^{14}C record. *Journal of Climate*, *17*(5), 1147–1156. https://doi.org/10.1175/1520-0442(2004)017<1147:SWMITS>2.0.CO;2

Guilderson, T. P., Schrag, D. P., Goddard, E., Kashgarian, M., Wellington, G. M., & Linsley, B. K. (2000). Southwest subtropical Pacific surface water radiocarbon in a high-resolution coral record. *Radiocarbon*, *42*(2), 249–256. https://doi.org/10.1017/S0033822200059051

Guilderson, T. P., Schrag, D. P., Kashgarian, M., & Southon, J. (1998). Radiocarbon variability in the western equatorial Pacific inferred from a high-resolution coral record from Nauru Island. *Journal of Geophysical Research*, *103*(C11), 24,641–24,650. https://doi.org/10.1029/98JC02271

Håkansson, S. (1983). University of Lund radiocarbon dates XVI. *Radiocarbon*, *25*(3), 875–891. https://doi.org/10.1017/S0033822200006263

Harkness, D. D. (1983). The extent of natural ^{14}C deficiency in the coastal environment of the United Kingdom, PACT. In W. G. Mook & H. T. Waterbolk (Eds.), *Proceedings of the First International Symposium ^{14}C and Archaeology: Groningen 1981*. Strasbourg: Council of Europe.

Harrison, P. J., Boyd, P. W., Varela, D. E., Takeda, S., Shiomoto, A., & Odate, T. (1999). Comparison of factors controlling plytoplankton productivity in the NE and NW subarctic Pacific gyres. *Progress in Oceanography*, *43*(2-4), 205–234. https://doi.org/10.1016/S0079-6611(99)00015-4

Hernandez-Guerra, A., & Joyce, T. M. (2000). Water masses and circulation in the surface layers of the Caribbean at 66°W. *Geophysical Research Letters*, *27*(21), 3497–3500. https://doi.org/10.1029/1999GL011230

Higham, T. F. G., & Hogg, A. G. (1995). Radiocarbon dating of prehistoric shell from New Zealand and calculation of the ΔR value using fish otoliths. *Radiocarbon*, *37*(2), 409–416. https://doi.org/10.1017/S0033822200030885

Hua, Q., Barbetti, M., & Rakowski, A. (2013). Atmospheric radiocarbon for the period 1950–2010. *Radiocarbon*, *55*(4), 2059–2072. https://doi.org/10.2458/azu_js_rc.v55i2.16177

Hua, Q., Woodroffe, C. D., Smithers, S. G., Barbetti, M., & Fink, D. (2005). Radiocarbon in corals from the Cocos (Keeling) Islands and implications for Indian Ocean circulation. *Geophysical Research Letters*, *32*, L21602. https://doi.org/10.1029/2005GL023882

Key, R. M. (1996). WOCE Pacific Ocean radiocarbon program. *Radiocarbon*, *38*(3), 415–423. https://doi.org/10.1017/S003382220003006X

Key, R. M., Kozyr, A., Sabine, C. L., Lee, K., Wanninkhof, R., Bullister, J. L., et al. (2004). A global ocean carbon climatology: Results from global data analysis project (GLODAP). *Global Biogeochemical Cycles*, *18*, GB4031. https://doi.org/10.1029/2004GB002247

Kong, G. S., & Lee, C. W. (2005). Marine reservoir corrections (ΔR) for southern coastal waters of Korea, the sea. *Journal of the Korean Society of Oceanography*, *10*(2), 124–128.

Konishi, K., Tanaka, T., & Sakanoue, M. (1982). Secular variation of radiocarbon concentration in sea-water: Sclerochronological approach. In E. D. Gomez (Ed.), *Proceedings of the fourth international coral reef symposium*, (Vol. 1, pp. 181–185). Manila: Marine Science Center, University of the Philippines.

Kubota, K., Shirai, K., Murakami-Sugihara, N., Seike, K., Minami, M., Nakamura, T., & Tanabe, K. (2018). Bomb-^{14}C peak in the North Pacific recorded in long-lived bivalve shells (Mercenaria stimpsoni). *Journal of Geophysical Research: Oceans*, *123*, https://doi.org/10.1002/2017JC013678, 2867–2881.

Kumamoto, Y., Murata, A., Kawano, T., Watanabe, S., & Fukasawa, M. (2013). Decadal changes in the bomb produced radiocarbon in the Pacific Ocean from the 1990s to 2000s. *Radiocarbon*, *55*(3), 1641–1650. https://doi.org/10.1017/S0033822200048554

Kumamoto, Y., Murata, A., Watanabe, S., & Fukasawa, M. (2007). Decadal changes of bomb radiocarbon in the subtropical South Pacific Ocean between 1992 and 2003. *Radiocarbon*, *49*(2), 937–945. https://doi.org/10.1017/S0033822200042806

Kumamoto, Y., Murata, A., Watanabe, S., & Fukasawa, M. (2011). Temporal and spatial variations in bomb-produced radiocarbon along BEAGLE2003 lines—Revisits of WHP P06, A10, and I03/I04 in the Southeren Hemisphere oceans. *Progress in Oceanography*, *89*(1-4), 49–60. https://doi.org/10.1016/j.pocean.2010.12.007

McFadgen, B. G., & Manning, M. R. (1990). Calibrating New Zealand radiocarbon dates of marine shells. *Radiocarbon*, *32*(2), 229–232. https://doi.org/10.1017/S0033822200040194

McNeely, R., Dyke, A. S., & Southon, J. R. (2006). Geological survey of Canada, Open File 5049, Canadian marine reservoir ages, preliminary data assessment, 3 pages.

Merino-Campos, V., de Pol-Holz, R., Southon, J., Latorre, C., & Collado-Fabbri, S. (2018). Marine radiocarbon reservoir age along the Chilean continental margin. *Radiocarbon*, *61*(1), 195–210. https://doi.org/10.1017/RDC.2018.81

Mitsuguchi, T., Dang, P. X., Kitagawa, H., Yoneda, M., & Shibata, Y. (2007). Tropical South China Sea surface ^{14}C record in an annually-banded coral. *Radiocarbon*, *49*(2), 905–914. https://doi.org/10.1017/S0033822200042776

Mitsuguchi, T., Hirota, M., Group, P. L. A. M. S. D., Yamazaki, A., Watanabe, T., & Yamano, H. (2016). Post-bomb coral $\Delta^{14}C$ record from Iki Island, Japan: Possible evidence of oceanographic conditions on the northern East China Sea shelf. *Geo-Marine Letters*, *36*(5), 371–377. https://doi.org/10.1007/s00367-016-0456-4

Mitsuguchi, T., Kitagawa, H., Matsumoto, E., Shibata, Y., Yoneda, M., Kobayashi, T., et al. (2004). High-resolution 14C analyses of annually-banded coral skeletons from Ishigaki Island, Japan: Implications for oceanography. *Nuclear Instruments and Methods in Physics Research, Section B: Beam Interactions with Materials and Atoms*, *223-224*, 455–459. https://doi.org/10.1016/j.nimb.2004.04.086

Morimoto, M., Kitagawa, H., Shibata, Y., & Kayanne, H. (2004). Seasonal readiocarbon variation of surface seawater recorded in a coral from Kikai Island, subtropical northwestern Pacific. *Radiocarbon*, *46*(2), 643–648. https://doi.org/10.1017/S0033822200035694

Nadal De Masi, M. A. (1999). Prehistoric hunter-gatherer mobility on the southern Brazilian coast: Santa Catarina Island, (PhD thesis, 186 p.), Stanford University.

Nydal, R., Brenkert, A. L., & Boden, T. A. (Eds.) (1998). *Carbon-14 Measurements in Surface Water CO_2 from the Atlantic, Indian and Pacific Oceans, 1965-1994. ORNL/CDIAC-104, NDP-057A* (pp. 131). Oak Ridge, TN: Carbon Dioxide Information Analysis Center, Oak Ridge National Laboratory. https://doi.org/10.3334/CDIAC/otg.ndp057

Olsen, A., Key, R. M., van Heuven, S., Lauvset, S. K., Velo, A., Lin, X., et al. (2016). The Global Ocean data analysis project version 2 (GLODAPv2)—An internally consistent data product for the world ocean. *Earth System Science Data*, *8*(2), 297–323. https://doi.org/10.5194/essd-8-297-2016

Petchey, F., Phelan, M., & White, J. P. (2004). New ΔR values for the southwest Pacific Ocean. *Radiocarbon*, *46*(2), 1005–1014. https://doi.org/10.1017/S0033822200036079

Qiu, B., Rudnick, D. L., Cerovecki, I., Cornuelle, B. D., Chen, S., Schönau, M. C., et al. (2015). The Pacific north equatorial current, new insights from the origins of the Kurhshio and Mindanao currents (OKMC) project. *Oceanography*, *28*(4), 24–33. https://doi.org/10.5670/oceanog.2015.78

Quinn, T. M., Taylor, F. W., Crowley, T. J., & Link, S. M. (1996). Evaluation of sampling resolution in coral stable isotope records: A case study using records from New Caledonia and Tarawa. *Paleoceanography*, *11*(5), 529–542. https://doi.org/10.1029/96PA01859

Robinson, S. W., & Thompson, G. (1981). Radiocarbon corrections for marine shell dates with application to southern Pacific northwest coast prehistory. *Syesis*, *14*, 45–57.

Sarmiento, J. L., Gruber, N., Brzezinski, M. A., & Dunne, J. P. (2004). High-latitude controls of thermocline nutrients and low latitude biological productivity. *Nature*, *427*(6969), 56–60. https://doi.org/10.1038/nature02127

Sherwood, O. A., Edinger, E. N., Guilderson, T. P., Ghaleb, B., Risk, M. J., & Scott, D. B. (2008). Late Holocene radiocarbon variability in Northwest Atlantic slope waters. *Earth and Planetary Science Letters*, *275*(1-2), 146–153. https://doi.org/10.1016/j.epsl.2008.08.019

Sprintall, J., Gordon, A. L., Koch-Larrouy, A., Lee, T., Potemra, J. T., Pujiana, K., & Wijffels, S. E. (2014). The Indonesian seas and their role in the coupled, ocean-climate system. *Nature Geoscience*, *7*(7), 487–492. https://doi.org/10.1038/ngeo2188

Stramma, L., Ikeda, Y., & Peterson, R. G. (1990). Geostrophic transport in the Brazil current region north of 20°S. *Deep Sea Research*, *37*(12), 1875–1886. https://doi.org/10.1016/0198-0149(90)90083-8

Tisnérat-Laborde, N., Montagna, P., McCulloch, M., Siani, G., Silenzi, S., & Frank, N. (2013). A high-resolution coral-based $\Delta^{14}C$ record of surface water processes in the Western Mediterranean Sea. *Radiocarbon*, *55*(3), 1617–1630. https://doi.org/10.1017/S0033822200048530

Tomczak, M., & Godfrey, J. S. (1994). *Regional oceanography: An introduction*, (p. 422). Oxford: Pergamon.

Wagner, A. J., Guilderson, T. P., Slowey, N. C., & Cole, J. E. (2009). Prebomb surface water radio-carbon of the Gulf of Mexico and Caribbean as recorded in hermatypic corals. *Radiocarbon*, *51*(3), 947–954. https://doi.org/10.1017/S0033822200034020

Weidman, C. R., & Jones, G. A. (1993). A shell-derived time history of bomb ^{14}C on Georges Bank and its Labrador Sea implications. *Journal of Geophysical Research*, *98*(C8), 14,577–14,588. https://doi.org/10.1029/93JC00785